described with a relatively simple initial structure in which, due to packing of the ions and the stresses resulting from this, a great number of structural deformations occur.

The authors wish to thank Professor R. Mańka for discussions and valuable comments during the preparation of the manuscript.

References

BECKMAN, O. & KNOX, K. (1961). *Phys. Rev.* **121**, 376–380.

BERNARD, D. J. & WALKER, W. C. (1976). *Rev. Sci. Instrum.* **47**, 122–127.

COX, U. J. (1989). *J. Phys. Condens. Matter*, **1**, 3565–3577.

GIBAUD, A., COWLEY, R. R. & NOUET, J. (1989). *Phase Transit.* **14**, 129–138.

GLAZER, A. M. (1972). *Acta Cryst.* B**28**, 3384–3392.

HIDAKA, M. (1975). *J. Phys. Soc. Jpn*, **39**, 180.

HIDAKA, M., FUJII, H. & MAEDA, S. (1986). *Phase Transit.* **6**, 101–114.

HIDAKA, M., OHAMA, N., OKAZAKI, A., SAKASHITA, H. & YAMAKAWA, S. (1975). *Solid State Commun.* **16**, 1121–1124.

ISING, E. (1925). *Z. Phys.* **31**, 253.

KASSAN-OGLY, F. A. & NAISH, V. E. (1986). *Acta Cryst.* B**42**, 297–335.

KNOX, K. (1961). *Acta Cryst.* **14**, 583.

LANDAU, L. D. & LIFSHITZ, E. M. (1964). *Statistical Physics.* Moscow: Nauka Press. [In Russian.]

LOCKWOOD, D. & TORRI, B. (1974). *J. Phys. C*, **7**, 2729–2744.

MINKIEWICZ, U. J., FUJII, Y. & YAMADA, Y. (1970). *J. Phys. Soc. Jpn*, **28**, 443.

MINKIEWICZ, U. J. & SHIRANE, G. (1969). *J. Phys. Soc. Jpn*, **26**, 674–680.

OKAZAKI, A. & SUEMUNE, Y. (1961). *J. Phys. Soc. Jpn*, **16**, 671.

RATUSZNA, A. & GLAZER, A. M. (1988). *Phase Transit.* **12**, 347–354.

RATUSZNA, A. & MAJEWSKA, K. (1990). *Powder Diffr.* **5**, 41–43.

REIFF, F. (1965). *Statistical and Thermal Physics.* New York: McGraw-Hill.

RESHCHIKOVA, L. M., ZINIENKO, W. J. & ALEKSANDROV, K. S. (1969). *Solid State Phys.* **11**, 3448–3454. [In Russian.]

SAKASHITA, H. & OHAMA, N. (1982). *Phase Transit.* **2**, 263–276.

SHIRANE, G. S., MINKIEWICZ, V. & LINZ, A. (1970). *Solid State Commun.* **8**, 1941.

STANLEY, H. E. (1971). *Introduction to Phase Transitions and Critical Phenomena.* Oxford: Clarendon Press.

Acta Cryst. (1992). B**48**, 122–134

Four-Dimensional Crystallographic Analysis of the Incommensurate Modulation in a $Bi_2Sr_2CaCu_2O_8$ Single Crystal

BY X. B. KAN AND S. C. MOSS

Physics Department and Texas Center for Superconductivity, University of Houston, Houston, TX 77204–5504, *USA*

(*Received* 12 *February* 1991; *accepted* 24 *September* 1991)

Abstract

The incommensurately modulated structure in single crystals of nominal composition $Bi_2Sr_2CaCu_2O_8$ has been solved with the aid of four-dimensional crystallography. 700 unique X-ray reflections were collected, including 265 fundamentals, 350 first-order and 85 second-order satellites. The overall weighted R factor (wR) is 0.073, while the partial wR values for fundamentals and first- and second-order satellites are 0.066, 0.086 and 0.133 respectively. Up to second-order harmonics were included in the modulation function along with the temperature factors, B_{ij}. In addition, Ca is partially replaced by Sr and Bi, and Sr sites have some vacancies; Bi has a large first- and second-order modulation of the B factor, which suggests a static disorder in the Bi sites; and the CuO_2 planes suffer a measurable modulation of their average structure. These findings are in fair agreement with earlier results by Petricek, Gao, Lee & Coppens [*Phys. Rev. B* (1990), **42**, 387–392]. However, our moduation amplitudes are in significant disagreement. A small c-axis component to the modulation wavevector was observed along with substantial disorder in the interplanar phasing of the modulation waves. Diffuse scattering at 'unallowed' Bragg positions was also measured.

Introduction

Following the observation of superconductivity at 20 K by Michel, Hervieu, Borel, Grandin, Deslandes, Provost & Raveau (1987) for the BiSrCuO system, the addition of Ca to this ternary system led Maeda, Tanaka, Fukutomi & Asano (1988) to the discovery of bulk superconductivity at 85 K and evidence of superconductivity at 110 K in the BiSrCaCuO system. The compound with a formal composition of $Bi_2Sr_2CaCu_2O_{8+x}$ (hereafter denoted Bi2212) was found to be responsible for superconductivity at 85 K in the Bi system and its basic structure was soon established (Tarascon, Le Page, Barboux,

0108-7681/92/020122-13$03.00

Bagley, Greene, McKinnon, Hull, Giroud & Hwang, 1988; Sunshine, Siegrist, Schneemeyer, Murphy, Cava, Batlogg, van Dover, Fleming, Glarum, Nakahara, Farrow, Krajewski, Zahurak, Waszczak, Marshall, Marsh, Rupp & Peck, 1988; Liang, Xie, Che, Huang, Zhang & Zhao, 1988). Tarascon, McKinnon, Barboux, Hwang, Bagley, Greene, Hull, Le Page, Stoffel & Giroud (1988) then isolated and identified three Bi-based cuprates of the general formula $Bi_2Sr_2Ca_{n-1}Cu_nO_{2n+4}$ with $n = 1$, 2 and 3, T_c being 10, 85 and 110 K, respectively. These three structures are basically similar. The perovskite-related slabs $SrO(CuO_2Ca)_{n-1}CuO_2SrO$, with different numbers of CuO_2Ca slabs stacked along the c axis, are separated by BiO double layers. The c parameters are about 24.6, 30.8 and 37.1 Å for $n = 1$, 2 and 3, respectively. The basic $n = 2$ structure is shown in Fig. 1, taken from Beskrovnyi, Dlouha, Jirak, Vratislav & Pollert (1990).

All three Bi phases possess an incommensurate modulation along the b axis ($b \simeq 5.4$ Å) with a period ~ 4.72 times b. A number of studies have focused on the average structure (Sunshine *et al.*, 1988; Hewat, Capponi & Marezio, 1989; Eibl, 1988). The earliest space-group assignment for the Bi2212 phase was *I4/mmm*, a tetragonal system with $a = 3.82$ Å (Tarascon, Le Page *et al.*, 1988; Liang *et al.*, 1988). However, *I4/mmm* was later found to be only approximate, because non-zero intensities were observed at forbidden reflections. Withers, Thompson, Wallenberg, Fitzgerald, Anderson & Hyde (1988) and Subramanian, Torardi, Calabrese, Gopalakrishnan, Morrisey, Askew, Flippen, Chowdhry & Sleight (1988) have determined an orthorhombic space group *Amaa* (where the a axis was chosen to be the direction of the modulation) with $a \simeq b \simeq 5.4$ Å. Petricek *et al.* (1990) chose a non-centrosymmetric space group *A2aa* based on their least-squares fitting. There have been a number of transmission electron microscopy (TEM) studies on the incommensurate modulation (Zandbergen, Groen, Mijlhoff, van Tendeloo & Amelinckx, 1988; Withers *et al.*, 1988; Hirotsu, Tomioka, Ohkubo, Yamamoto, Nakamura, Nagakura, Komatsu & Matsushita, 1988; Matsui, Maeda, Tanaka, Horiuchi, Takakawa, Takayama-Muormachi, Umezono & Ibe, 1988; van Tendeloo, van Landuyt & Amelinckx, 1988; Shindo, Hiraga, Hirabayashi, Kikuchi & Syono, 1988; Olivier, Groen, van der Beek & Zandbergen, 1989; Hewat *et al.*, 1989; Eibl, 1988) as well as a neutron powder diffraction study (Yamamoto, Onoda, Takayama-Muromachi, Izumi, Ishigaki & Asano, 1990) and a preliminary neutron single-crystal study on the modulated structure (Beskrovnyi *et al.*, 1990). Matsui *et al.* (1988) observed twinning and intergrowth faulting in the Bi2212 phase using TEM. More recently, the modulation waves at different layers along the c axis were found to suffer a random phase slip (Kan, Kulik, Chow, Moss, Yan, Wang & Zhao, 1990) as deduced from the broadening of the X-ray satellite reflections along the c axis.

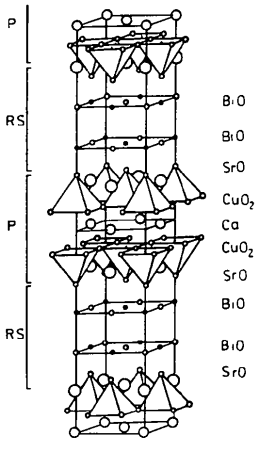

Fig. 1. The basic (unmodulated) structure for the $Bi_2Sr_2CaCu_2O_8$ crystal taken from Beskrovnyi *et al.* (1990). RS denotes the nominally rock-salt BiO layers while P refers to the perovskite blocks.

From their TEM images, Hirotsu *et al.* (1988) proposed a commensurate model for Bi2212 with the modulation period equal to five times the b parameter, in order to approximate the incommensurate modulation, where Bi double layers are observed to be buckled in the bc plane. Le Page, McKinnon, Tarascon & Barboux (1989) studied a system which is isostructural to Bi2212 in which Cu is replaced by Fe. The composition was $Bi_{10}Sr_{15}Fe_{10}O_{46}$. In this case the modulation was truly commensurate, with a period equal to five times the b parameter, and they used a conventional three-dimensional crystallographic method to solve its structure. They also found that the perovskite-related slabs as well as the Bi double layers were buckled. The structure of the two-dimensional BiO layers was described as roughly 70% of the rock-salt type and 30% of an oxygen-deficient perovskite type. They also conjectured that there were extra O atoms in the BiO layers which they proposed to account for the incommensurate modulation.

Yamamoto *et al.* (1990) included the incommensurate modulation in their Rietveld analysis of neutron and X-ray powder data on Bi2212, but due to the long period of the modulation, neighboring peaks were difficult to distinguish. Gao, Lee, Coppens, Subramanian & Sleight (1988) and Petricek *et al.* (1990) did X-ray studies on single crystals of Bi2212 using a four-dimensional crystallographic approach to solve the modulation structure. They found a large value of the temperature factor for Bi indicating some kind of static disorder. They

also observed that the oxygen displacement in the BiO layer varies linearly with the unit-cell position, with possibly an extra O atom present at the end of each modulation period. Their choice of superspace group was M:$A2aa$:$\bar{1}11$, a notation to which we shall return. Lee, Gao, Shen, Petricek, Restori, Coppens, Darovskikh, Phillips, Sleight & Subramanian (1989) did an anomalous X-ray scattering measurement at the Bi L_{III} absorption edge to study the Bi distribution over cation sites. They found that both Ca and Sr sites were partially occupied by Bi. In a related study Calestani, Rizzoli, Francesconi & Andreetti (1989) performed a single-crystal X-ray analysis on a nearly commensurate crystal of $Bi_2Sr_{3-x}Ca_xCu_2O_8$ with $\lambda \simeq 5a$. As with Le Page *et al.* (1989) they could therefore utilize a conventional three-dimensional crystallographic method to solve the superstructure. While we are sympathetic to their claim that the modulation is caused by a mismatch between perovskite and BiO layers, and not by insertion of extra O atoms, the present results on the actual incommensurate structure do not definitively resolve this issue.

Diffraction theory

The diffraction pattern of a one-dimensionally modulated structure consists of sharp spots where the diffraction vector **h** of each spot can be expressed by the reciprocal basis vectors **a***, **b*** and **c*** of the fundamental structure and a wavevector **q** of the modulation as

$$\mathbf{h} = h_1\mathbf{a}^* + h_2\mathbf{b}^* + h_3\mathbf{c}^* + h_4\mathbf{q} \qquad (1)$$

where h_1 to h_4 are integers commonly referred to as h, k, l, m (hkl are conventional Miller indices, m is the order of the satellite). The wavevector $\mathbf{q} = q_1\mathbf{a}^* + q_2\mathbf{b}^* + q_3\mathbf{c}^*$. The defining characteristic feature of an incommensurate structure is that at least one of the q_i values is irrational. In the case of the Bi2212 phase, $q_1 = 0$, $q_2 \simeq 0.212$ and is an irrational number, and $q_3 = 1$. q_2 was found to change continuously when Gd is doped onto the Ca sites (Kulik, Xue, Sun & Bonvalot, 1990); when the Sr/Ca ratio was changed (Calestani *et al.*, 1989), a nearly commensurate structure was obtained at $q_2 \simeq 0.2$. In the Bi2201 phase, q_2 increases from 0.192 to 0.238 as the Bi/Sr ratio increases (Hiroi, Ikeda, Takano & Bando, 1991). These results further support the true incommensurate character of the modulation (*i.e.* doping can continuously change q_2). In a one-dimensional displacively modulated structure (see Yamamoto, 1982*b*; Janssen & Janner, 1987), the positional vector of the μth atom in the nth unit cell (of the basic lattice) in three dimensions can be written as

$$\mathbf{r}_{n\mu} = \mathbf{n} + \mathbf{x}^\mu + \mathbf{u}^\mu[\mathbf{q}\cdot(\mathbf{n} + \mathbf{x}^\mu)] \qquad (2)$$

where **n** is the position of the nth unit cell, $\mathbf{x}^\mu$ is the average position of the μth atom in the unit cell, $\mathbf{u}^\mu[\mathbf{q}\cdot(\mathbf{n} + \mathbf{x}^\mu)]$ is the deviation of the μth atom in the nth unit cell from its average position, $\mathbf{u}^\mu(t + 1) = \mathbf{u}^\mu(t)$, and **q** is the modulation wavevector.

Based on the four-dimensional description, the structure factor of the four-dimensional unit cell can then be derived to be

$$F(\mathbf{h}') = \sum_{\mu(R|\tau)} f^\mu(\mathbf{h}) \int_0^1 d\bar{x}_4^\mu P^\mu(\bar{x}_4^\mu) \times \exp\left(-\sum_{ij=1}^{4} h_i[RB^\mu(\bar{x}_4^\mu)\tilde{R}]_{ij}h_j + 2\pi i \sum_{j=1}^{4} \{h_j[Rx^\mu(\bar{x}_4^\mu)]_j + h_j\tau_j\} \right) \qquad (3)$$

where **h** [given by (1)] is the projection of the four-dimensional reciprocal lattice vector $\mathbf{h}'$ ($= \sum_{i=1}^{4} H_i\mathbf{a}_i^*$) onto R_3, and $f^\mu(\mathbf{h})$ is the usual atomic scattering factor for the μth atom evaluated at the point **h** and μ runs over all non-equivalent atoms and $(R|\tau)$ runs over all symmetry operators in R_4 which generate new atoms from non-equivalent atoms. P^μ values are the occupational probabilities, B^μ are the anisotropic temperature-factor tensors.

Experimental techniques and results

Sample preparation

As $Bi_2Sr_2CaCu_2O_x$ cleaves so readily along basal planes, it is difficult to grow a good single crystal large enough for X-ray measurements. Usually the crystals exhibit a substantial mosaic spread, as well as intergrowth faulting (intimate mixture of $n = 1$, 2, 3 phases) or 90° domain rotations as observed by TEM (Matsui *et al.*, 1988) in which regions of the crystal alternate their a and b axes. The present crystal was from a batch provided by Yan, Li, Chu, Wang, Fung, Chang, Chen, Zheng, Mai, Yang & Zhao (1988) and its selection and X-ray characterization was reported by us earlier (Kan *et al.*, 1990). Similar crystals were also studied by Petricek *et al.* (1990) and our results are thus directly comparable.

X-ray crystallographic scans with a sealed-tube X-ray source

The integrated intensities of both fundamental, and first- and second-order reflections were collected in Houston with an automated 1/4-circle diffractometer with a sealed-tube Mo X-ray source monochromated for $K\alpha$ using highly oriented pyrolytic graphite. (The '1/4-circle' is actually a four-circle system with a χ range limited to between -10 and 100°.) A scintillation detector with wide-open (5 ×

5 mm) receiving slits was used in the ω-scan mode. The data were collected using the software *SUPER* written by Fleming (1985), later modified by Robertson (1989) and subsequently by Kan (1990).

The mosaic spread of our sample was 0.2° for the $0k0$ reflections and 0.18° for the $00l$ reflections. ω scans were done by fixing the 2θ (detector), χ and φ motors at the correct angles for a particular reflection, in the bisecting mode, and stepping the ω motor through the peak while counting.

The crystal was mounted inside a thin-walled (0.01 mm) quartz glass capillary. The size of the sample was about 1 × 0.3 × 0.02 mm, and the incident X-ray beam was collimated by a vertical and a horizontal slit to a size of 1.8 × 1.8 mm, thereby insuring that the sample was uniformly illuminated in all orientations. The glass capillary has negligible absorption for Mo $K\alpha$. However, the sample had appreciable absorption with $\mu_l t = 0.94$ for transmission normal to the sample plate and maximum and minimum transmission factors of 0.39 and 0.05 for our experiment. (This thickness actually gives nearly maximum diffracted intensities.) The orientation matrix was obtained by carefully locating 20 fundamental reflections. The final lattice constants are a = 5.415 (2), b = 5.421 (2), c = 30.88 (2) Å. The fractional indices h, $k + 0.212m$, $l + m$ (h, k, l, m are integers) were used to calculate the angle setting for the satellite reflection $hklm$.

Figs. 2(*a*), 2(*b*) and 2(*c*) are the ω scans for a fundamental, a first-order and a second-order satellite reflection. The scans cover a range of ±1.5° centred around the peak, which is sufficient to include most the mosaic blocks. A reference peak (0,0,20.0) was scanned after every 50 peak scans to check the stability of the X-ray source and the intensity variation of this reflection was less than 1% throughout the data collection. Each reflection was first scanned quickly to estimate its intensity; if it was too strong (beyond the linear region of the detector) or too weak (peak over background intensity is less than 25 c.p.s.), it was disregarded. (The ones that were too strong were measured later by putting some attenuators in the beam path.) Then a counting time was determined so that the total number of counts above background was about 10 000. Then the peak was rescanned using that counting time. The background was estimated using five data points on each end of a scan, the average of which gives a good estimate. This was then subtracted from each data point whose summation gives the integrated intensity. In total, about 3000 unique reflections were measured, of which 700 were sufficiently intense, including 265 fundamental reflections, 350 first-order and 85 second-order satellite reflections. The indices h, k run from 0 to 6; l from 0 to 30; m from −2 to 2. 2θ angles are between 10 and 80°. The data were corrected for several experimental factors: the amplitude of the structure factor, $|F_{obs}|$, is given by $|F_{obs}|$ = constant $(I_{obs}/LpA)^{1/2}$, where $L = 1/\sin(2\theta)$ is the Lorentz factor, p is a polarization factor $p = [1 + \cos^2(2\theta_g)\cos^2(2\theta)]$ where $\theta_g = 6.08°$ is the Bragg angle of the monochromator, and A is the absorption factor. Since the sample we used has the shape of a thin plate, in the case of transmission (diffracted beam on the opposite side of the sample from the incident beam),

$$A = \frac{\sin\theta_1 \sin\theta_2}{\mu t(\sin\theta_1 - \sin\theta_2)}\left[\exp\left(\frac{-\mu t}{\sin\theta_1}\right) - \exp\left(\frac{-\mu t}{\sin\theta_2}\right)\right],$$

and in the case of reflection (diffracted beam on the same side as the incident beam),

$$A = \frac{\sin\theta_1 \sin\theta_2}{\mu t(\sin\theta_1 + \sin\theta_2)}\left\{1 - \exp\left[\frac{\mu t(\sin\theta_1 + \sin\theta_2)}{\sin\theta_1 \sin\theta_2}\right]\right\},$$

where θ_1 and θ_2 are the angles between the sample basal plane and the incident and diffracted beams, respectively, and μt is the absorption coefficient multiplied by the thickness of the plate and was independently measured.

X-ray synchrotron (NSLS) line profile scans

The synchrotron radiation scans were done on the Oak Ridge National Laboratory beamline X14 at the Brookhaven National Synchrotron Light Source (NSLS). The double Si-111 monochromator crystals could be finely detuned by a piezo crystal attached to

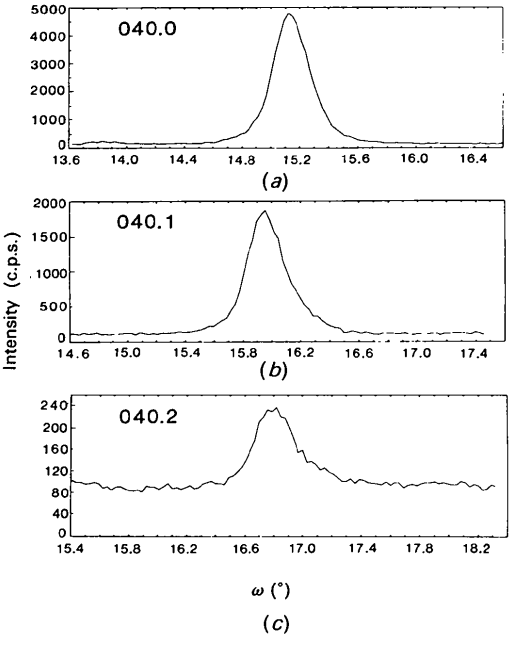

Fig. 2. Rocking curves (ω scans) of fundamental (*a*), first-order (*b*) and second-order (*c*) reflections; the intensities are directly comparable.

one of them in order to eliminate the $\lambda/3$ harmonic in the incident beam. The second of the two crystals was also segmented to provide sagittal focussing in the horizontal plane. A gas ionization chamber was placed before the entrance slits to monitor the main beam. A scintillation counter with a large dynamical range was used as the detector. The software *ORDIF* (unpublished) from the Oak Ridge National Laboratory controlled the experiment.

In order to reduce the background, the energy was selected at 8.7 keV, which corresponds to $\lambda =$ 1.42512 Å or just below the Cu absorption edge (= 8.98 keV). It should be noted that there will now be appreciable glass absorption compared to $\lambda =$ 0.7 Å. The receiving slit sizes were selected at 4 × 4 mm in order to accept scattering from most of the mosaic blocks while maintaining relatively high resolution.

The major results of these synchrotron radiation scans concern the nature of the defects and disorder in the crystal and will be separately treated in some detail in a later publication. They are included here in order to provide a more complete characterization. Figs. 3(*a*), 3(*b*), 3(*c*) show l scans along 04l.1, 04l.2 and 04l.3 satellite rows. Two features are clear in these scans: (*a*) the breadth in l (aside from mosaic spread effects near $l = 0$) increases with increasing satellite order, m, and this breadth is considerably greater than the fundamental peak width along l (Kan *et al.*, 1990); (*b*) there is a pronounced diffuse scattering at 'unallowed' positions ($h + l + m = 2n \pm 1$) whose intensity is not m dependent in any monotonic fashion and whose width is independent of m.†

The first of these effects implies a randomness in the phase modulation wave from layer to layer which must be seen in the context of a small deviation from 1.0 of the c^* component of the modulation wavevector. This c^* deviation was carefully measured at the NSLS to be about $-0.008m$ which means that the c^* component of **q** is actually $1 - 0.008 = 0.992$. In real space this implies a regular inclination of the stacking of the modulation waves toward one direction along the b axis, say the positive **b** direction. The amount of shift in real space along the b axis of the proposed antiphase points in adjacent Bi–perovskite–Bi slabs is Δb where $\Delta = 0.008/0.212 = 0.0377$. Δb is thus 0.2 Å for the amount of consistent progressive shift per slab for the modulation waves. In other words the modulation of the structure is not progressively stacked from layer to layer exactly 180° out-of-phase (Le Page *et al.*, 1989) but ~177.2° (see the schematic in Kan *et al.*, 1990); there is, in addition, some randomness on top of this progressive shift associated with the aforementioned m-dependent breadth of the satellites.

† A different l ($= l + m$) was used in this section and in Fig. 3.

The second of these effects, the diffuse scattering, is associated with small c-axis transverse-zone boundary displacements (in the **b** direction) of the basic structure weakly correlated (~80 Å) along **c**. Both of these stacking aspects (see Kan, 1990) will, as noted, be discussed in another report.

Results

Assignment of the basic space group and the superspace group

From the Laue and Buerger precession patterns of our Bi single crystal we determined (Kan *et al.*, 1990) that the diffraction pattern has the point-group symmetry *mmm* in reciprocal space; in agreement with other workers its Laue class is thereby found to be *mmm* and it is an orthorhombic system. The systematic extinction pattern of the fundamental reflections observed here is almost consistent with the basic space group *Bbmb* or *Bb2b* claimed by Withers *et al.* (1988) (in their notation it is *Amaa* or *A2aa*). Strictly speaking, however, the presence of

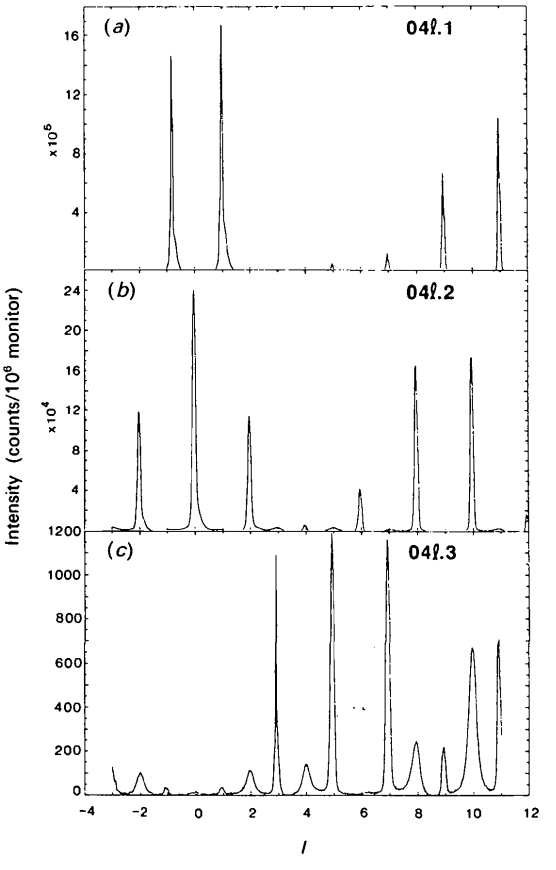

Fig. 3. l scans of first- (*a*), second- (*b*) and third-order (*c*) satellites taken at the Brookhaven NSLS. Note both the m-dependent widths of the sharp peaks and broader diffuse scattering at 'unallowed' positions ($h + l + m =$ odd).

extremely weak (sharp) peaks in both X-ray and electron diffraction patterns at, say, 030 and 050 violates the *b*-glide planes and lowers the symmety of the average structure to a highest possible space group *Bmmm*. However, for practical purposes the difference is negligible and the noncentrosymmetric *Bb2b*, also used by Petricek *et al.* (1990), is adopted in our analysis for the sake of simplicity.

We now turn to the superspace group. A thorough investigation of the four-dimensional superspace groups has been carried out by de Wolff, Janssen & Janner (1981) and revised by Yamamoto, Janssen, Janner & de Wolff (1985). They found that in total there are 775 four-dimensional superspace groups. According to de Wolff *et al.* (1981), the modulation wavevector $\mathbf{q}$ is first separated into its rational and irrational parts $\mathbf{q}_r$ and $\mathbf{q}_i$. In the case of Bi2212, $\mathbf{q}_r = \mathbf{c}^* = (0,0,1)$ and $\mathbf{q}_i = (0,0.212,0)$. The rotational part of the four-dimensional symmetry operator consists of a 3×3 block R and a 1×1 block ε in the diagonal direction. $R\mathbf{q}_i = \varepsilon\mathbf{q}_i$, $\varepsilon = \pm 1$.

In our case, $m_x\mathbf{q}_i = \mathbf{q}_i$, $2_y\mathbf{q}_i = \mathbf{q}_i$ and $m_z\mathbf{q}_i = \mathbf{q}_i$. Therefore all ε values are equal to 1. The general selection rules from observations are $h + l =$ even for hkl reflections; for $0kl$, $k =$ even; for $hk0$, $k =$ even. The superspace group compatible with these rules therefore is N^{Bb2b}_{111}, where the prefix N indicates $\mathbf{q}_r = (0,0,1)$, the top line *Bb2b* refers to the basic space group and bottom line 111 indicates the value of the ε's corresponding to each operator directly above. This N^{Bb2b}_{111} is equivalent to N^{Ccc2}_{111} in the paper by de Wolff *et al.* (1981), the only difference being the choice of **b** and **c**.

There are eight symmetry operators $(R|\tau)$ for this group. The $(0,0,0)^+$ set are $(E,1|0,0,0,0)$, $(\sigma_x 1|0,\frac{1}{2},0,0)$ $(c_{2y},1|0,0,0,0)$ and $(\sigma_z,1|0,\frac{1}{2},0,0)$. The $(\frac{1}{2},0,\frac{1}{2})^+$ set are obtained by multiplying the above four operators with the *B*-centering translational operator $(E,1|\frac{1}{2},0,\frac{1}{2},0)$. The two parts on the left-hand side of the vertical bar denote the three-dimensional rotation operator and ε respectively. E is the identity operator, σ_x, σ_y are the mirror planes normal to the a and c axes, c_{2y} is the twofold rotation about the b axis. The right-hand side is the translational part τ.

Results for the crystallographic parameters and chemical analysis

Based on the noncentrosymmetric superspace group N^{Bb2b}_{111} discussed above, the least-squares refinement was done using the program *REMOS* written by Yamamoto (1982*a*). The structure-factor formula used in *REMOS* was given in equation (3). Altogether, 700 unique reflections, including 265 fundamental reflections, 350 first-order and 85 second-order reflections, were used in the least-squares sum given by $S = \sum_i W_F^i(|F_{\rm cal}^i| - |F_{\rm obs}^i|)^2$,

Table 1. *Crystal data collection and structure refinement*

Formula (from microprobe analysis)	$Bi_{2.05\pm0.03}Sr_{1.98\pm0.01}Ca_{0.75\pm0.03}Cu_{2\pm0.04}O_{7.16\pm0.5}$
Radiation	Graphite-monochromatized Mo $K\alpha$
Unique reflections measured	3000
Observed	700
Absorption correction	Analytical
Basic space group	*Bb2b*
Superspace group	N^{Bb2b}_{111}
Lattice constants (Å)	$a = 5.415$ (2), $b = 5.421$ (2), $c = 30.88$ (2)
Formula units per unit cell	4
Number of parameters	166
Refinement	Full-matrix least-squares fit
Overall weighted R factor	0.073
Partial wR on fundamentals	0.066
First-order satellites	0.086
Second-order satellites	0.133
Atomic scattering factors	*International Tables for X-ray Crystallography*, (1974) Vol. IV)

where the proper weight W_F was $1/\sigma^2(|F_{\rm obs}|)$, which is proportional to $t(P_c - RT_b)/(P_c + R^2T_b)$ where t is the counting time, and P_c is the total counts under the peak. T_b represents the total counts in the two background regions and R is the ratio of the length of peak region to the background region. The integrals in the structure factor were calculated numerically by use of the Gauss method in the program. Up to second-order harmonics were included in the modulation function as well as the temperature factors, B_{ij}'s. The crystal data collection and structural refinement are summarized in Table 1.

In order to determine the chemical composition, electron microprobe analysis on several samples from the same crystal batch was done at the Electron Microprobe Laboratory of the Texas Center for Superconductivity at the University of Houston. A sheet-like single crystal was cleaved to reveal a fresh flat surface which was then pasted on a carbon disk. Care was taken to insure that the probing electron beam was perpendicular to the surface to produce a reliable result. Three points on the sample were measured, with fairly consistent results. The average composition of these three points was $Bi_{2.05\pm0.03}Sr_{1.98\pm0.01}Cu_{2\pm0.04}Ca_{0.75\pm0.03}O_{7.16\pm0.5}$ (normalized to Cu_2). The deficiency in Ca is quite reliable, and it is confirmed by our crystallographic analysis as well as by Petricek *et al.* (1990). However, the value of the oxygen content has a large error due to the fact that the light O atoms are sited among the heavy-metal elements. Our X-ray crystallographic analysis also shows that Bi is present at other metal-atom sites. The Bi valence is generally believed to be +3. Ren, Whangbo, Tarascon, Le Page, McKinnon & Torardi (1989) did a tight-binding electronic band structure calculation on the BiO double layer, using the commensurate modulated structure model by Le Page *et al.* (1989) for the $Bi_{10}Sr_{15}Fe_{10}O_{46}$ system, and they found that because of the presence of short Bi—O bonds, the Bi 6*p*-block bands lie above the

Fermi level, so that the formal oxidation state for Bi is indeed +3.

Both Sr and Ca have +2 valence, and if the oxygen content is ideal (=8), the composition in Table 1 will give a formal valence of +2.19 to Cu. However, the exact oxygen composition is difficult to determine either by electron microprobe or by the X-ray diffraction technique due to the low atomic number of oxygen. The ideal composition for oxygen (8) was used throughout the subsequent analysis. Neutron scattering, of course, is sensitive to oxygen and we have attempted a single-crystal neutron study at the Intense Pulsed Neutron Source at the Argonnne National Laboratory. Unfortunately, our largest single-crystal sample was not big enough to yield a reliable data set.

The valence of 2.19 for Cu noted above is in good agreement with several authors' estimates for the Bi2212 superconductor. Our X-ray analysis shows consistently that Bi and Cu sites are fully occupied, while 11% of the Sr sites are vacant. Ca sites are partially replaced by heavier elements, either Sr or Bi, or both. Unfortunately, the *REMOS* program is only capable of dealing with two species on any given type of site. Therefore, we tried Sr on the Ca site first, which results in 41% Sr and 59% Ca, but this Ca content is unreasonably low. We then tried Bi on the Ca site resulting in 11% Bi and 89% Ca in which case the Ca content is too high. Since Bi is heavier than Sr, and from the electron microprobe result the overall Ca content is 0.75, which is in between the two cases, our analysis therefore implies that both Bi and Sr are distributed on the Ca site. Petricek *et al.* (1990) have an earlier X-ray determination for the Ca site: 6% Bi, 19% Sr, 75% Ca. Their composition was $Bi_{2.15}Sr_{1.92}Ca_{0.75}Cu_2O_{8.1}$.

The least-squares X-ray structure refinement with fixed positions and the ideal composition ($Bi_2Sr_2CaCu_2O_8$) converged, yielding a weighted R factor $wR = (R_t|R_0,\ R_1,\ R_2) = (0.105|0.091,\ 0.135,\ 0.149)$, where R_0, R_1, R_2 are defined by $\{\sum_h W_F(h)[|F_{obs}(h)| - |F_{cal}(h)|]^2/\sum_h W_F(h)|F_{obs}(h)|^2\}^{1/2}$ for the fundamental reflections, first-order and second-order satellite reflections, respectively; R_t is the overall R factor. A significant improvement of agreement was achieved by refining the oxygen positions with $wR = (0.0841|0.066,\ 0.117,\ 0.151)$. As the temperature factors (B factor) for the O atoms were not refinable, an isotropic B factor of 1 Å^2 for the O atoms was used throughout the fits. Anisotropic B factors were used for all the metal atoms, with modulation up to second order on the B factor for Bi. The fits were quite insensitive to the substitutional (compositional) modulations. Next, Sr was introduced into the Ca site and the optimum fit was 40% Sr and 60% Ca on Ca sites with $wR = (0.0851|0.069,\ 0.116,\ 0.137)$. Then an alternative choice was made, where 13% of Sr sites were vacant and 11% of Ca sites were occupied by Bi with $wR = (0.082|0.065,\ 0.115,\ 0.134)$. The refinement on the modulation of the substitutional probability again yielded little improvement. A third alternative of 25% Sr on Ca sites and 13% vacancy on Sr leads to $wR = (0.082|0.065,\ 0.113,\ 0.137)$, so the electron microprobe results on composition were more reliable. Our best estimate of the composition is $Bi_{2.05}Sr_{1.98}Ca_{0.75}Cu_2O_8$. The site occupancies are listed in Table 2.

Table 2. *Site occupancies*

Ca/Ca	0.75 ± 0.05
Sr/Ca	0.2 ± 0.05
Bi/Ca	0.05 ± 0.03
Cu/Cu	1*
Sr/Sr	0.89 ± 0.05
Vacancy/Sr	0.11 ± 0.05
Bi/Bi	1*
O/O	1*

* Parameters were not refined.

All the above analyses were done strictly according to superspace group N^{Bb2b}_{111}. This imposes a twofold axis (c_{2y}) on Ca sites, and the symmetry thereby requires that $c_{2y}\mathbf{u}^{Ca}(t) = \mathbf{u}^{Ca}(t)$, therefore $u_x^{Ca}(t) = u_z^{Ca}(t) = 0$, implying that there is no displacive modulation of Ca along the a and c axes. However, this was physically unrealistic, since the neighboring CuO_2 layers on both sides are appreciably modulated along the c axis and the interlayer interaction will thus make the Ca layer buckle in the c direction as well. In addition, as we noted earlier, the basic space group $Bb2b$ is only approximate and the true space group belongs to a lower, possibly monoclinic, system. Therefore both a- and c-axis modulations in addition to the b-axis modulation, were introduced on the Ca site, which lead to significant improvement in the first-order satellite R factor with $wR = (0.073|0.066,\ 0.086,\ 0.133)$. The final crystallographic parameters are listed in Table 3 along with the Fourier amplitudes of the modulation which are in significant disagreement with Petricek *et al.* (1990) even though the average structures agree rather well (see Table 3). The fractional coordinates x, y, z are obtained by $x(t) = x_o + c_1^*\cos 2\pi t - s_1^*\sin 2\pi t + c_2^*\cos 4\pi t - s_2^*\sin 4\pi t$, *etc.* The second-harmonic terms, $c_2^*\cos 4\pi t - s_2^*\sin 4\pi t$, were found to be quite important; fitting by first-harmonic terms alone yielded $wR = (0.091|0.068,\ 0.114,\ 0.28)$ and the fit on second-order satellites significantly deteriorated. Table 4 lists the minimum and maximum nearest-neighbor interatomic distances.†

† A list of structure factors with their e.s.d.'s has been deposited with the British Library Document Supply Centre as Supplementary Publication No. SUP 54603 (11 pp.). Copies may be obtained through The Technical Editor, International Union of Crystallography, 5 Abbey Square, Chester CH1 2HU, England.

Fig. 4 shows (100), (010) and (001) projections of the modulated structure in which the modulations are appreciable at all layers. Roughly speaking, it is a sinusoidal buckling of the Bi–perovskite–Bi slabs stacked in a nearly antiphase configuration, as was found by Le Page *et al.* (1989) in the case of an Fe-based commensurate analog, and by several other authors (Hirotsu *et al.*, 1988; Calestani *et al.*, 1989; Petricek *et al.*, 1990). The layers of the perovskite-related slab ($SrO–CuO_2–Ca–CuO_2–SrO$) bend together elastically, the Ca layer in the middle having the least tension and in-plane deformation, while the SrO layer on the outside has the most tension and in-plane deformation. These effects can be seen easily when viewing Fig. 4 along the c axis. Notice also that the Bi atoms move off the atomic rows along the c axis two or three times every modulation period λ (= 25.5 Å, about nine or ten rows), which results from the lattice mismatch between the BiO double layer and the perovskite-related slab.

Fig. 5 shows the projection along the c axis of each layer while Figs. 6 and 7 show the metal–metal and metal–oxygen nearest-neighbor distances respectively as a function of phase t. The most striking feature is the Bi—O double-chain formation (Fig. 5*d*) as proposed by Le Page *et al.* (1989). The nearest Bi—Bi

Table 3. *Final crystallographic parameters*

The number in parentheses is the uncertainty of the last one or two digits.

Positional and thermal parameters ($\times 10^3$) of the average structure (isotropic B_{iso} for O atoms in Å^2)

	x	y	z	B_{11}/B_{iso}	B_{22}	B_{33}	B_{23}	B_{31}	B_{12}
Present results									
Ca	0.25*	0*	0.25*	0 (9)	0 (6)	0.0 (3)	−1 (1)	−1 (1)	−2 (4)
Cu	0.2501 (8)	0.499 (7)	0.1962 (2)	5 (3)	7 (3)	0.2 (1)	2 (1)	−0.7 (8)	−4 (6)
Sr	0.2524 (8)	−0.003 (7)	0.1395 (2)	1 (2)	2 (3)	0.0 (1)	1.7 (6)	0.0 (6)	−4 (7)
Bi	0.2251 (4)	0.483 (6)	0.0514 (1)	11 (1)	30 (2)	0.0 (1)	1.7 (6)	0.3 (4)	−7 (4)
O(1)	−0.01 (2)	0.75 (2)	0.196 (1)	1*					
O(2)	0.49 (3)	0.27 (3)	0.196 (2)	1*					
O(3)	0.42 (1)	0.56 (2)	0.102 (3)	1*					
O(4)	0.04 (1)	0.21 (2)	0.057 (3)	1*					
Petricek *et al.* (1990)									
Ca	0.250	0	0.2500	5 (3)	9 (3)	21 (5)	0	−2 (7)	0
Cu	0.2499 (6)	0.500	0.1965 (1)	−1 (3)	10 (2)	23 (3)	0	−4 (4)	0
Sr	0.2525 (5)	0	0.1408 (1)	5 (2)	23 (2)	21 (2)	0	5 (3)	0
Bi	0.2337 (5)	0.505 (2)	0.0523 (9)	21 (2)	71 (3)	13 (2)	−8 (4)	−4 (2)	10 (4)
O(1)	0	0.75	0.197 (1)	10					
O(2)	0.50	0.25	0.199 (1)	10					
O(3)	0.289 (6)	0.53 (2)	0.116 (1)	10					
O(4)	0.157 (5)	0.02 (2)	0.056 (2)	10					

Amplitudes of the positional ($\times 10^3$) and thermal parameter modulations ($\times 10^3$)

	Fourier term	x	y	z	B_{11}	B_{22}	B_{33}	B_{23}	B_{31}	B_{12}
Present results										
Ca	C1	0 (4)	0 (5)	8 (1)						
	S1	5 (7)	6 (8)	−7 (2)						
	C2	−4 (17)	−4 (7)	−2 (2)						
	S2	42 (8)	7 (8)	4 (2)						
Cu	C1	2 (5)	−6 (6)	9.4 (5)						
	S1	1 (9)	16 (2)	−2 (2)						
	C2	−4 (14)	2 (7)	−3 (1)						
	S2	−14 (7)	2 (4)	−3 (2)						
Sr	C1	−2 (5)	−29 (5)	8.6 (4)						
	S1	−5 (11)	47 (3)	4 (1)						
	C2	−9 (11)	13 (5)	−1.5 (6)						
	S2	−7 (9)	−12 (4)	0 (1)						
Bi	C1	4 (3)	−43 (5)	4.0 (5)	−2 (2)	−26 (5)	0.0 (1)	−2.0 (8)	0.1 (5)	11 (5)
	S1	3 (3)	59 (3)	4.2 (5)	−4 (4)	−12 (5)	−0.1	−0.6 (5)	−0.3 (5)	9 (3)
	C2	3 (5)	8 (2)	−5.8 (7)	3 (4)	15 (6)	0.1 (1)	1.5 (5)	0.2 (4)	3 (3)
	S2	−2 (6)	−10 (4)	2 (1)	2 (5)	14 (4)	0.0 (1)	0.8 (8)	0.5 (5)	0 (6)
O(1)	C1	30 (40)	3 (40)	10 (4)						
	S1	−10 (20)	6 (20)	11 (8)						
	C2	−6 (48)	−38 (36)	2 (6)						
	S2	31 (39)	−12 (45)	−2 (10)						
O(2)	C1	24 (43)	41 (48)	9 (6)						
	S1	12 (21)	11 (19)	−16 (7)						
	C2	5 (44)	11 (10)	−1 (6)						
	S2	−6 (29)	16 (42)	−2 (14)						
O(3)	C1	−18 (19)	−101 (23)	9 (4)						
	S1	8 (24)	146 (26)	−13 (5)						
	C2	80 (18)	27 (26)	16 (4)						
	S2	−91 (21)	12 (24)	7 (4)						
O(4)	C1	53 (17)	73 (21)	−2 (5)						
	S1	132 (15)	−98 (18)	−8 (5)						
	C2	−23 (18)	133 (19)	−24 (4)						
	S2	41 (20)	30 (23)	4 (5)						

* Parameters were not refined.

Table 3 (*cont.*)

	Fourier term	x	y	z	B_{11}	B_{22}	B_{33}	B_{23}	B_{31}	B_{12}
Petricek *et al.* (1990)										
Ca	C1	2 (9)	0	8.4 (3)						
	S1	0	0	0						
	C2	0	0	0						
	S2	0	7 (4)	0						
Cu	C1	6 (4)	0	−9.0 (3)						
	S1	0	−11 (11)	0						
	C2	15 (6)	0	−2.3 (3)						
	S2	0	2 (2)	0						
Sr	C1	7 (5)	0	−6.8 (3)						
	S1	0	−41 (2)	0						
	C2	4 (7)	0	−2.3 (7)						
	S2	0	−19 (2)	0						
Bi	C1	−7 (2)	15 (4)	−30 (2)	1 (4)	51 (6)	−5 (2)	−7 (3)	6 (5)	19 (6)
	S1	−11 (2)	−61 (2)	2 (2)	−25 (4)	33 (4)	−4 (5)	4 (5)	2 (2)	8 (3)
	C2	−20 (2)	−2 (4)	−11 (2)	−14 (4)	54 (4)	−8 (4)	−1 (6)	−5 (6)	21 (6)
	S2	−2 (4)	−17 (2)	11 (2)	−5 (6)	14 (9)	−1 (5)	30 (3)	−28 (3)	−21 (6)
O(1)	C1	0	0	−8.7 (3)						
	S1	−10 (30)	0	0						
	C2	0	0	0						
	S2	−2 (22)	7 (4)	0						
O(2)	C1	0	0	−20 (17)						
	S1	−9 (28)	−11 (17)	0						
	C2	0	0	50 (13)						
	S2	7 (20)	−11 (13)	0						
O(3)	C1	15 (11)	43 (20)	−11 (2)						
	S1	−6 (30)	−83 (11)	−2 (4)						
	C2	24 (15)	20 (22)	−7 (3)						
	S2	−4 (26)	−54 (13)	5 (4)						

Table 4. *Nearest-neighbour interatomic distances* (Å)

Element	Bond	Minimum	Maximum
Ca—Ca	1	3.58 ± 0.05	4.10 ± 0.05
	2	3.54 ± 0.05	4.12 ± 0.05
Cu—Cu	1	3.73 ± 0.05	3.93 ± 0.05
	2	3.72 ± 0.05	3.99 ± 0.05
Sr—Sr	1	3.70 ± 0.05	4.06 ± 0.05
	2	3.65 ± 0.05	4.08 ± 0.05
Bi—Bi	1	3.47 ± 0.05	3.88 ± 0.05
	2	3.88 ± 0.05	4.31 ± 0.05
Ca—Cu	1	2.94 ± 0.05	3.40 ± 0.05
	2	3.00 ± 0.05	3.30 ± 0.05
	3	2.88 ± 0.05	3.50 ± 0.05
	4	2.92 ± 0.05	3.42 ± 0.05
Cu—O	1	1.60 ± 0.2	2.30 ± 0.2
	2	1.60 ± 0.2	2.10 ± 0.2
	3	1.50 ± 0.2	2.10 ± 0.2
	4	1.70 ± 0.2	2.40 ± 0.2
	5	2.30 ± 0.2	4.20 ± 0.2
Sr—O	1	2.70 ± 0.2	4.30 ± 0.2
	2	1.50 ± 0.2	3.10 ± 0.2
	3	2.40 ± 0.2	3.50 ± 0.2
	4	3.14 ± 0.2	4.70 ± 0.2
	5	2.10 ± 0.2	4.60 ± 0.2
Bi—O	1	1.10 ± 0.2	3.10 ± 0.2
	2	1.80 ± 0.2	2.70 ± 0.2
	3	2.40 ± 0.2	5.30 ± 0.2
	4	3.20 ± 0.2	5.30 ± 0.2
	5	2.60 ± 0.2	4.80 ± 0.2
	6	1.00 ± 0.2	2.80 ± 0.2

distances have separated into a long and a short branch (Fig. 6*d*), the shorter branch being within the double Bi chain while the longer branch connects two such chains. The O atoms are confined within each chain, but fluctuate strongly about the average position. However, the oxygen positions are not really reliable, due to the intensitivity of the X-rays to oxygen, and they therefore should not be taken too seriously. As in Le Page *et al.* (1989), they can be roughly sorted into an oxygen-deficient perovskite type, where oxygen bridges two Bi atoms, and a rock-salt type, where oxygen resides at the idealized positions in Fig. 1 with Bi—Bi distances being longer in the perovskite region. As the bridging O atoms are closer to the Bi atoms (~1.9 Å) than in the rock-salt region, Bi is pushed further apart by the bridging O atoms (Fig. 6*e*). Bi atoms are in a favorable stereochemical environment, having three short Bi—O bonds roughly in three perpendicular directions {two of which are in the chain, while the third is connected to oxygen in the Sr–O layer [O(3)]} and three long Bi—O bonds (two of which are connected to O atoms in the neighboring Bi double chains and one is connected to the next Bi–O layer, Fig. 7*c*).

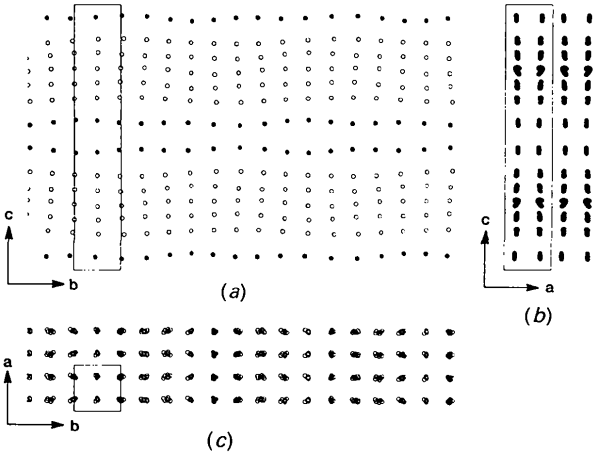

Fig. 4. (*a*) 100, (*b*) 010 and (*c*) 001 projections of the real-space (three-dimensional) modulated structure. The average unit cell is outlined and only metal atoms are shown. In (*a*) the solid circles are Bi atoms.

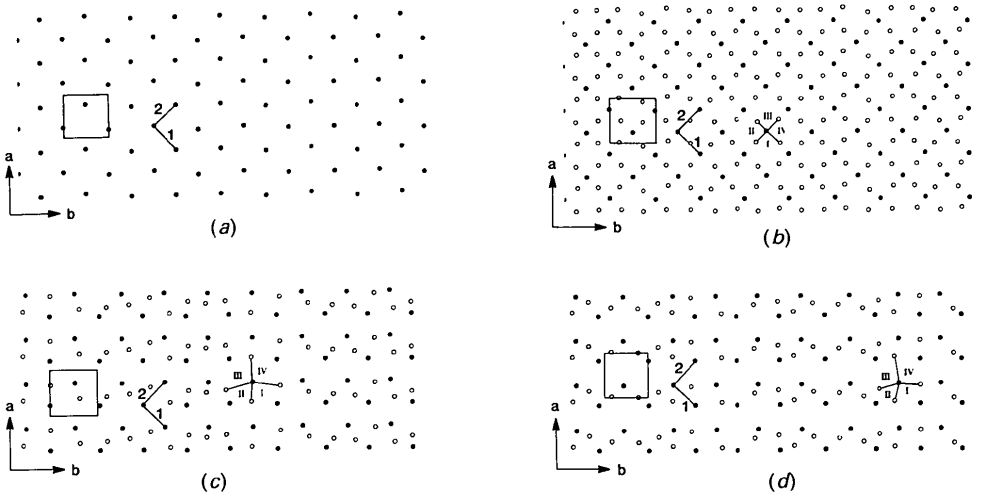

Fig. 5. Separate 001 projections of the (*a*) Ca, (*b*) CuO_2, (*c*) SrO and (*d*) BiO layers; notations 1 and 2 refer to nearest-neighbor metal–metal distances (see Fig. 6); notations I–IV refer to nearest-neighbor metal–oxygen distances (see Fig. 7).

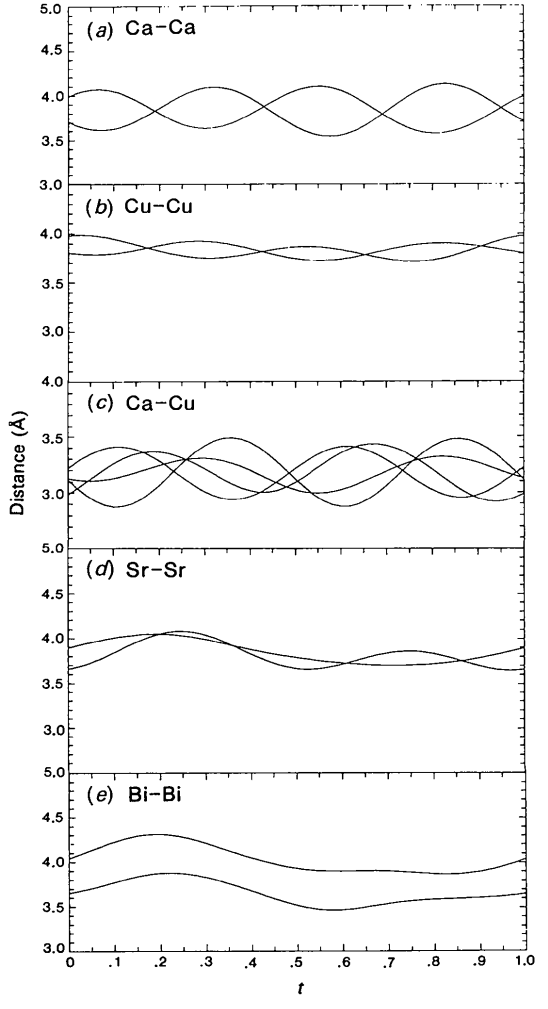

Fig. 6. (*a*)–(*e*) Nearest-neighbor metal-atom distances plotted over a full modulation period, $0 \le t \le 1.0$.

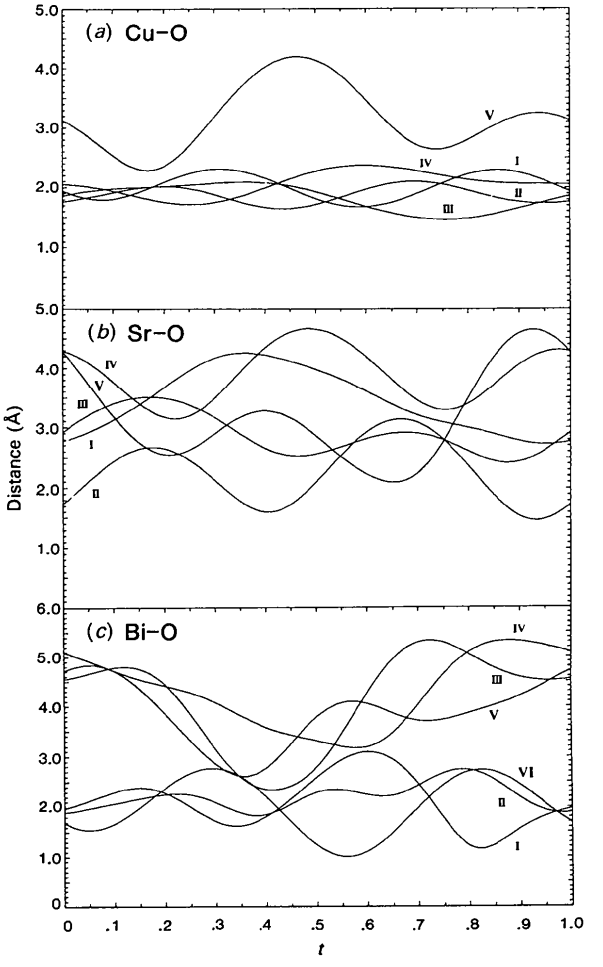

Fig. 7. (*a*)–(*c*) Nearest-neighbor metal–oxygen distances plotted over a full modulation period, $0 \le t \le 1.0$.

The CuO_2 plane is the least modulated, see Figs. 5(*b*), 6(*b*) and 7(*a*). The Cu—Cu distances vary between 3.7 and 4 Å, close to the Cu—Cu distance (~3.8 Å) in other Cu-perovskite materials such as $YBa_2Cu_3O_{7-x}$ and La_2CuO_4. The Cu—O distance varies between 1.5 ± 0.05 and 2.4 ± 0.05 Å. The in-plane square configuration for Cu—O was approximately maintained. The Ca plane was the second least modulated (Figs. 5*a* and 6*a*). These facts, taken together, support the idea that the perovskite-related slab is considerably stiffer than the Bi–O layers, and thus the mutual intermodulation mainly involves the Bi–O layer modulated by the perovskite-related slab, where Bi–O undergoes a large distortion to accommodate the perovskite in-plane lattice spacing. The Sr–O layer, however, was largely modulated on the O atoms (Figs. 5*c*, 6*c* and 7*b*), primarily due to interaction with the neighboring Bi–O layer, which is strongly modulated.

The anisotropic B factor for Bi along the b axis, B_{22}, was very large. From Table 3, $B_{22} = 0.03 - 0.002\cos 2\pi t + 0.004\sin 2\pi t + 0.003\cos 4\pi t - 0.002\sin 4\pi t$. The maximum is at $t = 0.3$, where $B_{22} = 0.08$; this corresponds to a large r.m.s. vibrational amplitude of 0.35 Å $[= b/\pi(B_{22}/2)^{1/2}]$ along the b axis. This is qualitively the same as the finding by Petricek *et al.* (1990). Such a large B factor of Bi implies that the Bi atomic positions suffer large fluctuations about their statistical average position as in equation (2). This fluctuation could be dynamic or static in nature. It occurs roughly where the Bi—Bi interatomic distance reaches a maximum, which is the oxygen-deficient perovskite region of the Bi–O layer. The minimum of B_{22} is at $t \simeq 0.6$, with $B_{22} = 0.004$, or 0.077 in Å which is the rock-salt region. Apparently the Bi–O coordination in the rock-salt region represents a stronger bonding than the Bi–O coordination in the oxygen-deficient perovskite-like region.

Discussion

The incommensurate modulation structure in a Bi2212 single crystal has been analyzed and described in four-dimensional space. Owing to the complexity of the chemical bonding in the Bi2212 material, the real symmetry is very low. Owing to the displacive modulation of Ca along the a and c axes, the symmetry must be lower than orthorhombic and could be monoclinic, with the a axis as the special axis, or even triclinic. Such a deviation from the orthorhombic symmetry is, nonetheless, very small. We also found that the modulation waves at neighboring Bi–perovskite–Bi slabs are not stacked exactly 180° out of phase on average, but $177.2 \pm 0.2°$ instead. This further supports the idea that the true symmetry is lower than orthorhombic. The deviation from the symmetric configuration is 2.8° in phase, or 0.2 ± 0.01 Å in real space. This preferential shift towards one direction breaks the symmetry between $+$ and $-b$ directions. This means that the interaction between the modulation waves at neighboring Bi–O layers (which is weakly ionic in nature) is itself asymmetric in the two directions. The asymmetry of the interaction arises from the fact that the modulation wavefield at each Bi–O layer is not symmetric in $+$ and $-b$ axis due to the higher-order harmonics in the modulation function. In our analysis, up to second-order harmonics were included. In reality, the modulation waves must include higher harmonics, as is clearly suggested by a poor agreement at $m = 3$ for the synchrotron radiation l scans using a structure factor with only two harmonics (Kan, 1990). The interaction between the two modulation waves in neighboring Bi–O layers, which depends on the actual form of the modulation waves, must therefore be asymmetric.

Origin of the modulation

An incommensurate modulation is a common phenomenon in hetero-layered structures. Well known examples include graphite intercalation compounds (see the review by Moss & Moret, 1989) and certain minerals. The modulation arises from the in-plane lattice spacing mismatch between the constituent layer components. The modulation period often changes continuously with a change in composition, sometimes resulting in a commensurate superstructure. Examples include $Bi_{10}Sr_{15}Fe_{10}O_{46}$ ($\lambda = 5a$) (Le Page *et al.*, 1989), $Bi_2Sr_{3-x}Ca_xCu_2O_y$ ($4.72a \leq \lambda \leq 5a$) (Calestani *et al.*, 1989), $Bi_2Sr_2(Ca_{1-x}Gd_x)Cu_2O_y$ ($4.1a \leq \lambda \leq 4.7a$) (Kulik *et al.*, 1990), where the a axis is along the modulation wave. Usually, in a two-component system, one type of layer or a group of layers (slab) is stiffer than the other type of layer/slab. The stiffer type largely preserves its original structure. In other words, it is not heavily modulated. The stiffer type is often referred to as the host layer. On the other hand, the weaker layers undergo a large modulation to accommodate the host-layer structure. They are often referred to as intercalant. Alkali–graphite intercalation compounds are good examples. The graphite sheets (host) are stronger than the alkali sheets (intercalant); therefore, at low temperature, the intercalant atoms order into a two-dimensionally incommensurate modulated structure, while the graphite layers remain essentially intact with only a small transverse distortional response.

The Bi-based perovskite systems fall conceptually somewhat into this class. The two constituents are the Bi–O layers and the perovskite-related slabs (Sr–Cu–Ca–Cu–Sr) with the latter as the dominant (stiffer) one. In fact, the CuO_2 plane changes only a

little from the original perovskite structure aside from its out-of-plane buckling (Figs. 4 and 5*a*) while the Bi–O layer undergoes large distortions and is rather ill defined, as evidenced from the large B factors of Bi. The Bi atoms may in fact have several different sites to randomly choose from.

The 25% deficiency of Ca of our sample, which was supported by the result of Sunshine *et al.* (1988) and Petricek *et al.* (1990), has raised the formal valence of Cu to about 2.2 even without any extra oxygen. None of these studies, however, can definitively answer this question of additional oxygen, mainly because the X-ray method is insufficiently sensitive to the oxygen content. The appreciable modulation may well result from the lattice mismatch between the Bi–O layers and perovskite-related slabs, as is often the case for hetero-layered structures where two competing interactions with different length scales exist. This point of view has been recently put forth by Gai, Subramanian & Sleight (1990) in their study of cation defects and oxygen interstitials in the Bi2212 materials. The extra O atom on the Bi–O layer, if any, may then be a consequence, rather than the cause, of the modulation. An alternative explanation is, of course, electronic in nature. However, it is quite unlikely that a charge-density-wave instability is important here as the modulation would seem to be too strong for that.

So far, all known classes of Cu-based high-T_c superconductors have an orthorhombic unit cell. Even for $YBa_2(Cu_{3-x}M_x)O_{7+\delta}$ $(0.12 < x < 0.4)$, where the average structure is tetragonal, local orthorhombic ordering has been observed for M = Al (Jiang, Wochner & Moss, 1990). The formation of the Bi-double chain here appears to be responsible for the orthorhombicity in the Bi-based structures (*i.e.* from a tetragonal perovskite structure to a B-centered orthorhombic structure). Whether there is some fundamental relationship between the orthorhombicity [even if it is weak, *i.e.* $(b-a)/a \ll 1$] and the high-T_c superconductivity is not clear at the moment.

This work was supported by the National Science Foundation on DMR-8903339 and the State of Texas at the Texas Center for Superconductivity at the University of Houston. We thank P. C. Chow for assistance in the early phase of these experiments and acknowledge with pleasure the availability of *REMOS* from Y. Yamamoto. We also thank G. E. Ice for assistance at the X14 beamline at the NSLS.

References

Beskrovnyi, A. I., Dlouha, M., Jirak, Z., Vratislav, S. & Pollert, E. (1990). *Physica*, C**166**, 79–86.

Calestani, C., Rizzoli, C., Francesconi, M. G. & Andreetti, G. D. (1989). *Physica*, C**161**, 598–606.

Eibl, O. (1988). *Solid State Commun.* **67**, 703–706.

Fleming, R. M. (1985). Unpublished.

Gai, P. L., Subramanian, M. A. & Sleight, A. W. (1990). Program Mater. Res. Soc. Fall Meet. p. 381.

Gao, Y., Lee, P., Coppens, D., Subramanian, M. A. & Sleight, A. W. (1988). *Science*, **241**, 954–956.

Hewat, E. A., Capponi, J. J. & Marezio, M. (1989). *Physica*, C**157**, 502–508.

Hiroi, Z., Ikeda, Y., Takano, M. & Bando, Y. (1991). *J. Mater. Res.* **6**, 435–445.

Hirotsu, Y., Tomioka, O., Ohkubo, T., Yamamoto, N., Nakamura, Y., Nagakura, S., Komatsu, T. & Matsushita, K. (1988). *Jpn. J. Appl. Phys.* **27**, L1869–L1872.

Janssen, T. & Janner, A. (1987). *Adv. Phys.* **36**, 519–624.

Jiang, X. G., Wochner, P. & Moss, S. C. (1990). Unpublished.

Kan, X. B. (1990). PhD Thesis, Univ. of Houston, USA.

Kan, X. B., Kulik, J., Chow, P. C., Moss, S. C., Yan, Y. F., Wang, J. H. & Zhao, Z. X. (1990). *J. Mater. Res.* **5**, 731–736.

Kulik, J., Xue, Y. Y., Sun, Y. Y. & Bonvalot, M. (1990). *J. Mater. Res.* **5**, 1625–1638.

Lee, P., Gao, Y., Shen, H. S., Petricek, V., Restori, R., Coppens, P., Darovskikh, A., Phillips, J. C., Sleight, A. W. & Subramanian, M. A. (1989). *Science*, **244**, 62–63.

Le Page, Y., McKinnon, W. R., Tarascon, J. M. & Barboux, P. (1989). *Phys. Rev. B*, **40**, 6810–6816.

Liang, J. K., Xie, S. S., Che, G. C., Huang, J. Q., Zhang, Y. L. & Zhao, Z. X. (1988). *Mod. Phys. Lett.* B**2**, 483–489.

Maeda, H., Tanaka, Y., Fukutomi, M. & Asano, T. (1988). *Jpn. J. Appl. Phys.* **27**, L209–L210.

Matsui, Y., Maeda, H., Tanaka, Y., Horiuchi, S., Takekawa, S., Takayama-Muormachi, E., Umezono, A. & Ibe, K. (1988). *JEOL News*, E**26**, 36–41.

Michel, C., Hervieu, M., Borel, M., Grandin, A., Deslandes, F., Provost, J. & Raveau, B. (1987). *Z. Phys.* B**68**, 421–423.

Moss, S. C. & Moret, R. (1989). *Springer Series in Materials Science*, Vol. 14, pp. 5–58. New York: Springer-Verlag.

Olivier, S., Groen, W. A., van der Beek, C. & Zandbergen, H. W. (1989). *Physica*, C**157**, 531–536.

Petricek, V., Gao, Y., Lee, P. & Coppens, P. (1990). *Phys. Rev. B*, **42**, 387–392.

Ren, J., Whangbo, M. H., Tarascon, J. M., Le Page, Y., McKinnon, W. R. & Torardi, C. C. (1989). *Physica*, C**158**, 501–506.

Robertson, J. L. (1989). Unpublished.

Shindo, D., Hiraga, K., Hirabayashi, M., Kikuchi, M. & Syono, Y. (1988). *Jpn. J. Appl. Phys.* **27**, L1018–L1021.

Subramanian, M. A., Torardi, C. C., Calabrese, J. C., Gopalakrishnan, J. K., Morrisey, K. J., Askew, T. R., Flippen, R. B., Chowdhry, U. & Sleight, A. W. (1988). *Science*, **239**, 1015–1017.

Sunshine, S. A., Siegrist, T., Schneemeyer, L. F., Murphy, D. W., Cava, R. J., Batlogg, B., van Dover, R. B., Fleming, R. M., Glarum, S. H., Nakahara, S., Farrow, R., Krajewski, J. J., Zahurak, S. M., Waszczak, J. V., Marshall, J. H., Marsh, P., Rupp, L. W. Jr & Peck, W. F. (1988). *Phys. Rev. B*, **38**, 893–896.

Tarascon, J. M., Le Page, Y., Barboux, P., Bagley, B. G., Greene, L. H., McKinnon, W. R., Hull, G., Giroud, M. & Hwang, D. M. (1988). *Phys. Rev. B*, **37**, 9382–9389.

Tarascon, J. M., McKinnon, W. R., Barboux, P., Hwang, D. M., Bagley, B. G., Greene, L. H., Hull, G. W., Le Page, Y., Stoffel, N. & Giroud, M. (1988). *Phys. Rev. B*, **38**, 8885–8892.

Tendeloo, G. van, van Landuyt, J. & Amelinckx, S. (1988). *JEOL News*, E**26**, 32–35.

Withers, R. L., Thompson, J. G., Wallenberg, L. R., Fitzgerald, J. D., Anderson, J. S. & Hyde, B. G. (1988). *J. Phys. C*, **21**, 6067–6083.

Wolff, P. M. de, Janssen, T. & Janner, A. (1981). *Acta Cryst.* A**37**, 625–636.

YAMAMOTO, A. (1982*a*). Unpublished.
YAMAMOTO, A. (1982*b*). *Acta Cryst.* A**38**, 87–92.
YAMAMOTO, A., JANSSEN, T., JANNER, A. & DE WOOLFF, P. M. (1985). *Acta Cryst.* A**41**, 418–530.
YAMAMOTO, A., ONODA, M., TAKAYAMA-MUROMACHI, E., IZUMI, F., ISHIGAKI, T. & ASANO, H. (1990). *Phys. Rev. B*, **42**, 4228–4239.
YAN, Y. F., LI, C. Z., CHU, X., WANG, J. H., FUNG, K. K., CHANG, Y. C., CHEN, G. H., ZHENG, D. N., MAI, Z. H., YANG, Q. S. & ZHAO, Z. X. (1988). *Mod. Phys. Lett.* B**2**, 571–575.
ZANDBERGEN, H. W., GROEN, W. A., MIJLHOFF, F. C., VAN TENDELOO, G. & AMELINCKX, S. (1988). *Physica*, C**156**, 325–354.

Acta Cryst. (1992). B**48**, 134–144

$La_{1.16}Mo_8O_{16}$: a Hollandite-Related Compound with an Incommensurate Modulated Structure

BY H. LELIGNY, PH. LABBÉ, M. LEDÉSERT AND B. RAVEAU

Laboratoire CRISMAT, ISMRa, Bd du Maréchal Juin, 14050 *Caen CEDEX, France*

AND C. VALDEZ AND W. H. MCCARROLL

Chemistry Department, Rider College, POB 6400, *Lawrenceville, NJ* 08648, *USA*

(*Received* 24 *April* 1991; *accepted* 1 *November* 1991)

Abstract

The hollandite-related structure $La_{1.16}Mo_8O_{16}$, M_r = 1184.66, tetragonal, $P4/1$, $a = 9.983$ (1), c = 2.8890 (5) Å, $V = 287.9$ Å^3, $Z = 1$, $D_x = 6.83$ g cm^{-3}, λ(Mo $K\alpha$) = 0.71069 Å, $\mu = 126$ cm^{-1}, $F(0000)$ = 530, room temperature, $R = 0.041$ for 1145 unique reflections with $I \geq 3\sigma(I)$. At room temperature the compound exhibits a one-dimensional incommensurate modulated structure with a modulation wavevector $\mathbf{q}^* = 0.608\,(1)\mathbf{c}^*$. Both a displacive modulation wave, acting on La, Mo and O atoms, and a modulation wave governing the occupancy probability of La sites inside the tunnels are involved in the crystal. Within the superspace group $P4/1$, the final R values of main reflections (477) and first- and second-order satellite reflections (523 and 145) are 0.030, 0.050 and 0.133 respectively. The more spectacular modulation features are the occurrence of La—La pairs in the tunnels and the formation of Mo_3 triangular clusters in the double chains of edge-sharing octahedra. Contrary to previous descriptions based upon rigid tunnels in structures of the hollandite type, the tunnels in the crystal studied are distorted in a periodic way along [001] (λ = 4.75 Å), giving rise to alternate contractions and expansions. The distortion of the double octahedral chains is considerable and probably created *via* the La—O(1) bonds by insertion of La atoms inside two adjacent tunnels.

Introduction

Oxides with the hollandite structure, corresponding to the general formula $A_xM_8O_{16}$ (A = Ba, Pb, K, Rb, Tl, Na; M = Ti, Mn, Fe, Mg, Mo...) form a large family and have been extensively studied for both their ionic conductivity and as encapsulants for radioactive waste. The structural principle of these materials is well established since many structure determinations of synthetic and mineral hollandites have been performed by means of X-ray and neutron diffraction; see, for instance, Sinclair, McLaughlin & Ringwood (1980), Torardi & McCarley (1981), Post, Von Dreele & Buseck (1982), Sinclair & McLaughlin (1982), Torardi & Calabrese (1984), Vicat, Fanchon, Strobel & Tran Qui (1986), Cheary & Squadrito (1989) and Cheary (1990). These oxides have also been studied by electron diffraction and high-resolution microscopy (Bursill & Grzinic, 1980; Mijlhoff, Ijdo & Zandbergen, 1985; Xiang, Fan, Wu, Li & Pan, 1990).

At first sight the $[M_8O_{16}]_\infty$ host lattice is very simple. It consists of infinite rutile chains sharing the edges and the corners of their MO_6 octahedra and forming large square tunnels where the A cations are located. In general, however, the actual structure of these compounds is more complex than can be described by these basic structural principles. A great number of these oxides exhibit superstructures, which have not yet been completely elucidated. This is the case for instance for the non-stoichiometric hollandites $Ba_xTi_{8-x}Mg_xO_{16}$ and $Ba_xTi_{8-2x}Ga_{2x}O_{16}$ with $0.8 < x < 1.33$ (Bursill & Grzinic, 1980), which exhibit a continuous variation of superlattice periodicity and multiplicity. Very complex phenomena can occur as shown by the recent electron diffraction study of the mineral ankangite $Ba_{0.8}(Ti,V,Cr)_8O_{16}$ by Xiang *et al.* (1990). These authors have shown that

0108-7681/92/020134-11$03.00